MATERIALS CHARACTERIZATION 61 (2010) 1245–1251

available at www.sciencedirect.com

ScienceDirect

www.elsevier.com/locate/matchar

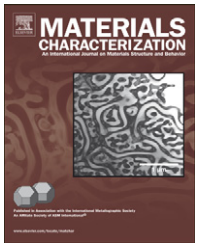

Transmission electron microscopy investigation of acicular ferrite precipitation in γ′-Fe_4N nitride

X.C. Xiong[a,b,*], A. Redjaïmia[b], M. Gouné[b,c]

[a]Shanghai Key Laboratory of Materials Laser Processing and Modification, School of Materials Science and Engineering, Shanghai Jiao Tong University, Shanghai 200240, China
[b]Institut Jean Lamour, UMR 7198 CNRS, Nancy-Universite, UPV-Metz, Ecole des Mines de Nancy, Parc de Saurupt CS 14234, F-54042 Nancy Cedex, France
[c]ArcelorMittal SA, Voie Romaine, BP 30320, F-57283 Maizières-lès-Metz, France

ARTICLE DATA

Article history:
Received 5 July 2010
Received in revised form
12 August 2010
Accepted 17 August 2010

Keywords:
Iron alloys
Acicular ferrite
Electron diffraction
Precipitation
Fe–N

ABSTRACT

Acicular-shaped crystals precipitate from γ'-Fe_4N nitride in an iron–nitrogen alloy and were identified by electron microdiffraction as α-ferrite. Acicular ferrite develops both the Nishiyama–Wassermann and the Kurdjumov–Sachs orientation relationships with γ'-Fe_4N nitride. These orientation relationships were discussed in terms of the symmetry theory. The driving force for acicular ferrite formation was related to the increasing nitrogen content of γ'-Fe_4N, in equilibrium with α-ferrite, with decreasing temperature. The passage from lamellar to acicular structure in Fe–N system was proposed.

1. Introduction

The iron–nitrogen system, similar to the iron–carbon system, undergoes a eutectoid reaction, which leads to the decomposition of austenite to α-ferrite and γ'-Fe_4N nitride at the eutectoid point (592 °C, 2.4 wt.%) [1–5]. The eutectoid product, labelled nitrogen pearlite [6–8], is similar to carbon pearlite.

In this study, pure iron specimens were nitrided in the austenite phase and then cooled very slowly in the furnace. In addition to nitrogen pearlite [8] which formed logically according to the Fe–N phases diagram, an acicular structure was also found in the specimens. This structure has not been reported and the mechanism of the phase transformation is not yet understood.

In order to elucidate what phases this "strange" acicular structure consist of and to understand the mechanism of the formation of this structure, electron microscopy and diffraction were used to reveal the morphology of the acicular structure, to determine the crystal structure (space group) of phases and orientation relationships between phases.

2. Experimental

Pure iron sheets of 0.75 mm thickness were nitrided at 840 °C for 120 min in ammonia–hydrogen gas mixtures, the composition of which was NH_3:H_2 = 1.3%:98.7% [5]. After nitriding, the specimens were maintained at 840 °C for 100 min to allow a uniform nitrogen distribution and were cooled slowly in the furnace (the approximate cooling rate was 10 °C/min). The nitrogen content (around 0.2 wt.%) was controlled and measured by a thermobalance

* *Corresponding author*. Shanghai Key Laboratory of Materials Laser Processing and Modification, School of Materials Science and Engineering, Shanghai Jiao Tong University, Shanghai 200240, China. Tel.: +86 21 34203743; fax: +86 21 54745526.
E-mail addresses: xiaochuan.xiong@sjtu.edu.cn, xiaochuan.xiong@gmail.com (X.C. Xiong).

1044-5803/$ – see front matter © 2010 Elsevier Inc. All rights reserved.
doi:10.1016/j.matchar.2010.08.005

equipped in the nitriding furnace and confirmed by chemical analysis. The nitrogen distribution homogeneity was checked by Vickers hardness tests and metallographic observations.

Optical and Scanning Electron Microscopy (SEM) observations were made by etching the specimen surface in a solution the composition of which is 0.5% hydrofluoric acid – 1% sulfuric acid – 98.5% distilled water. The preparation of thin foil specimens for Transmission Electron Microscopy (TEM) examination was achieved by using the double-jet technique with a 95% glacial acetic acid–5% perchloric acid electrolyte and finished by an ionic bombardment using small attack angles for 1 h. The Transmission Electron Microscopy used in this investigation is the Philips CM12 operated at 120 kV.

3. Results

3.1. *Morphology of the Acicular Structure*

According to the eutectoid point (2.4 wt.%, 592 °C) of the iron–nitrogen system, the nitrogen content of the alloy (0.2 wt.%) corresponds to a hypoeutectoid composition. Fig. 1 shows a typical hypoeutectoid structure, which is composed of proeutectoid ferrite and eutectoid products, the latter forming small islands distributed uniformly in the former. Two kinds of structures were observed on the islands (Fig. 2): the lamellar pearlitic structure [7,8], which is the compound of alternated lamellae of ferrite and of γ'-Fe_4N nitride, and the acicular structure the morphology of which is totally different from that of pearlite.

Figs. 3 and 4 clearly reveal the morphology of this acicular structure. Unlike pearlite in which all lamellae (α-ferrite and γ'-Fe_4N) grow in the same direction and are almost all parallel, the acicular structure is, to some extent, similar to acicular ferrite growing in austenite matrix.

By applying electron microdiffraction, it is now clear that the matrix is not austenite but γ'-Fe_4N nitride [8]. The dark-field imaging (Fig. 4b) shows that all γ'-Fe_4N nitrides are illuminated (all oriented in the same direction) and form a whole "block".

The acicular crystals have two different morphologies: small lenses and long platelets. Two pairs of V-shaped lenses

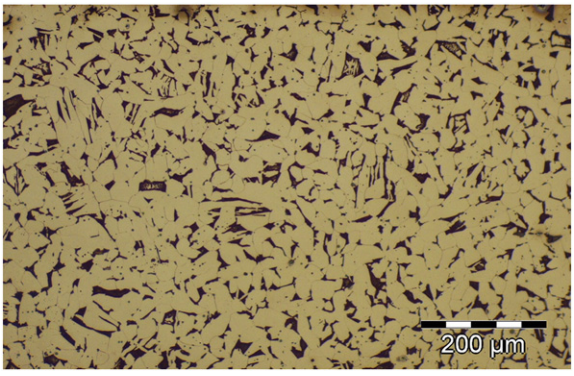

Fig. 1 – Optical micrograph of the slow cooled Fe-0.2wt.%N specimen showing a typical hypoeutectoid structure, a mixture of proeutectoid ferrite (bright parts) and eutectoid decomposition products (dark parts).

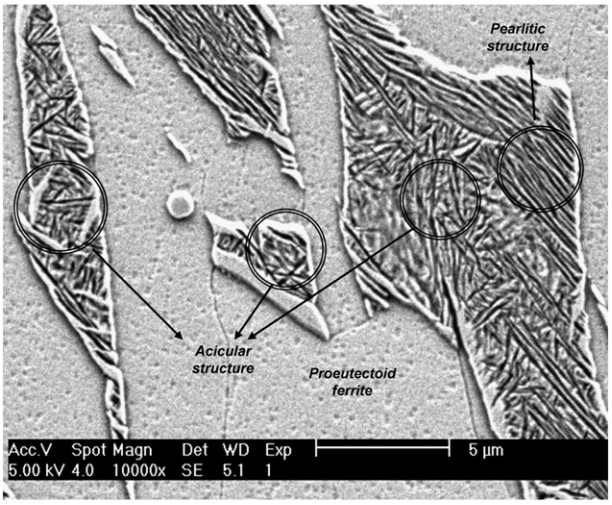

Fig. 2 – SEM micrograph showing both pearlitic and acicular structures.

are highlighted by the arrows in Fig. 2. The fact that two "V" have the same included angle and are arranged in the same direction strongly suggests that the acicular crystals develop orientation relationships with respect to the γ'-Fe_4N nitride.

Now the acicular structure can be described as "the acicular crystals developed in the γ'-Fe_4N matrix", and focus should be made on the identification of these acicular crystals.

3.2. *Identification of the Acicular Phases*

In order to identify the crystal structure of the acicular crystals, a series of Transmission Electron Microscopy investigations was

Fig. 3 – Bright-field TEM micrograph of acicular structure. Two pairs of lens-shaped crystals are highlighted by the arrows.

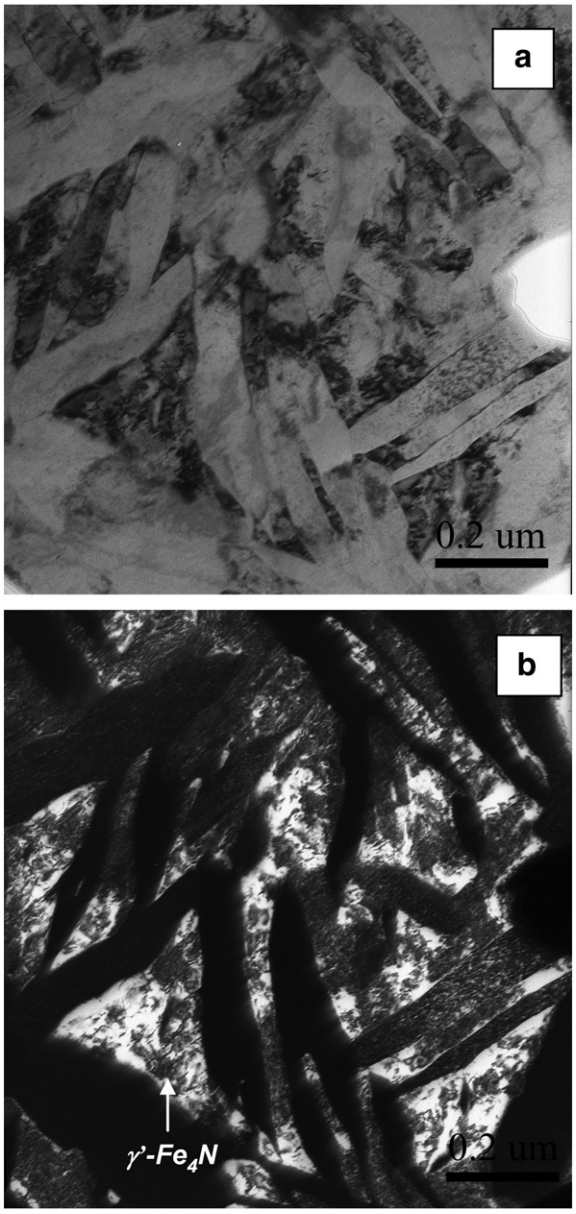

Fig. 4 – a) Bright-field and b) dark-field TEM micrographs of acicular structure, in the latter γ'-Fe_4N phase is illuminated.

conducted by applying a systematic microdiffraction method (Fig. 5) developed by Morniroli and Steeds [9,10]. The procedure of this characterization is briefly presented as follows:

1. The "net" symmetries for the Zero Order Laue Zones recorded along ⟨001⟩ and ⟨111⟩ zone axes exhibit (4 mm) and (6 mm) (Fig. 5), respectively. These "net" symmetries correspond to a cubic system;
2. The shift and the periodicity difference between the Zero Order Laue Zones and High Order Laue Zone reflection nets along ⟨001⟩ and ⟨011⟩ zone axes are related to the extinction symbol (Fig. 5), which may be associated with six spaces groups;
3. The "ideal" Zero Order Laue Zones symmetries correspond to (4 mm), (2 mm) and (6 mm) along ⟨001⟩, ⟨011⟩and ⟨111⟩ zone axes (Fig. 5), respectively. These "ideal" symmetries lead to the point group.

This procedure leads to the conclusion that the space group of the present crystals is $Im\bar{3}m$, or $I\frac{4}{m}\bar{3}\frac{2}{m}$ in its full crystallographic notation. From the $I\frac{4}{m}\bar{3}\frac{2}{m}$ space group and the lattice parameter $a=0.287$ nm, it is concluded without any ambiguity, that the acicular crystals are nothing but α-ferrite, no matter their shape is lens-like or platelet-like.

3.3. *Orientation Relationship Between Acicular Ferrite and γ'-Fe_4N Nitride*

Several electron diffraction patterns were recorded in order to reveal the orientation relationships between acicular α-ferrite and γ'-Fe_4N nitride. Diffraction patterns recorded along <011> direction (Figs. 6 and 7), from the same γ'-Fe_4N nitride block, point out the Nishiyama–Wassermann orientation relationship for platelet-like acicular ferrite and Kurdjumov–Sachs orientation relationship for lens-like acicular ferrite, respectively. These orientation relationships could be written as follows:

$$(011)\alpha//(111)\gamma';[100]\alpha//[1\bar{1}0]\gamma';[0\bar{1}1]\alpha//[\bar{1}\bar{1}2]\gamma' \text{ Nishiyama} - \text{Wassermann}$$

$$(011)\alpha//(\bar{1}\bar{1}1)\gamma';[11\bar{1}]\alpha//[1\bar{1}0]\gamma';[\bar{2}1\bar{1}]\alpha//[112]\gamma' \text{ Kurdjumov} - \text{Sachs}$$

Fig. 7 exhibits three reciprocal space nets: one of them corresponds to the γ'-Fe_4N nitride and the two others belong to acicular ferrite. The two acicular ferrite nets are related by a small rotation around the <111> zone axis. This rotation, estimated as 7°, is a deviation from the exact Kurdjumov–Sachs orientation relationship.

4. Discussion

4.1. *Morphology and Orientation Relationships*

It is interesting to relate the morphology to the orientation relationships on the basis of the symmetry theory [11,12]:

The intersection point group $H=G^{\alpha}\cap G^{\gamma'}$ is defined by the elements which are common to the point group G^{α} of acicular ferrite and the point group $G^{\gamma'}$ of γ'-Fe_4N nitride. For the Nishiyama–Wassermann and Kurdjumov–Sachs orientation relationships, the intersection point group H is $\frac{2}{m}$ and $\bar{1}$, respectively. This result is in agreement with Transmission Electron Microscopy observations and is analysed as follows:

- The point group $H=\frac{2}{m}$ (Nishiyama–Wassermann), corresponding to prismatic shape, exhibits long platelet forms as shown in Fig. 2,
- The point group $H=\bar{1}$ (Kurdjumov–Sachs), one of the least symmetric point groups, is consistent with pinacoid shape. This point group corresponds to short lens shape as marked by the arrows in Fig. 2.

This is also the reason why small departure (<7°) from the exact Kurdjumov–Sachs orientation relationship was

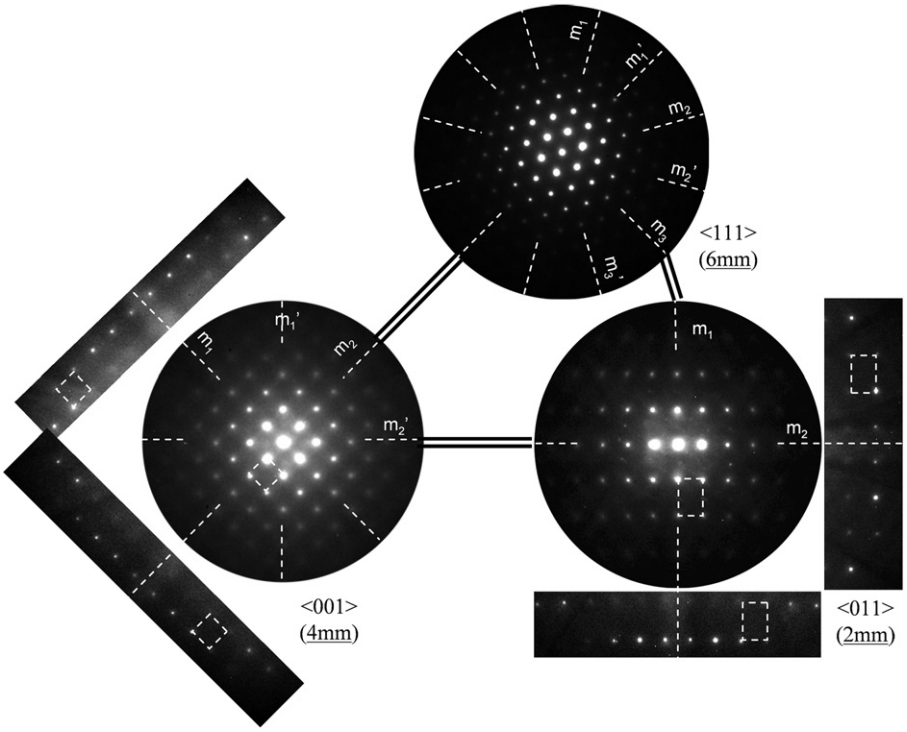

Fig. 5 – Series of microdiffraction Zone Axes Patterns (Zero Order Laue Zone and First Order Laue Zone) of acicular crystals revealing $I\frac{4}{m}\bar{3}\frac{2}{m}$ space group.

recorded. In fact, the Kurdjumov–Sachs orientation relationship is not energetically stable because the corresponding intersection point group $H = \bar{1}$ dictates no energy extremun [11].

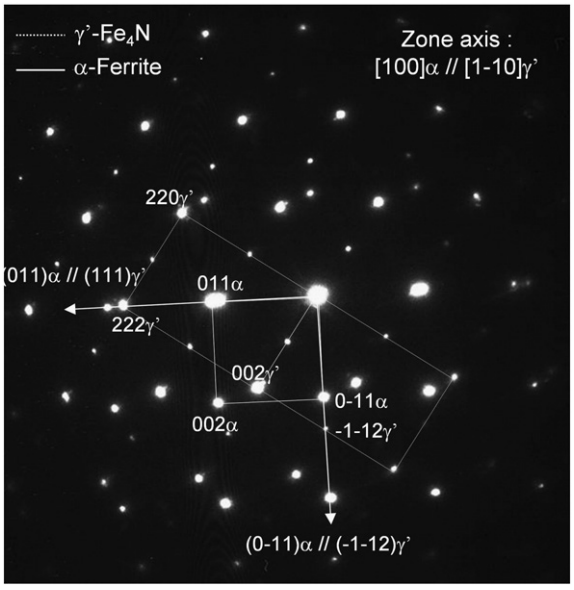

Fig. 6 – Electron diffraction pattern showing the Nishiyama–Wassermann orientation relationship between acicular ferrite and γ'-Fe_4N nitride. The arrows point out the characteristic parallelisms of this orientation relationship.

4.2. *Formation of Acicular Ferrite*

The formation of acicular ferrite could be understood by taking a close look at the iron–nitrogen phases diagram. In fact, γ'-Fe_4N nitride is non-stoichiometric and its crystallographic and thermodynamic details should be considered.

The ideal crystal lattice of stoichiometric γ'-Fe_4N can be considered as iron atoms arranged according to a Face Centered Cubic lattice containing a fully ordered distribution of nitrogen atoms at positions of the type (1/2, 1/2, 1/2) in the unit cells. But a defect structure can comprise either the presence of nitrogen atoms at positions of the type (1/2, 0, 0) and/or nitrogen vacancies at (1/2, l/2, 1/2). Consequently, the defect structure may be associated with the presence of excess nitrogen or the occurrence of nitrogen deficiency with respect to the stoichiometric composition (20 at.% or 5.88 wt.%N) and the non-stoichiometric nitride may be written as γ'-Fe_4N_{1-x} [3,13–16]. The nitrogen content of γ'-Fe_4N, in equilibrium with α-ferrite, increases as the temperature decreases, as shown in a schematic representation of the α+ γ'/γ' phase boundary in the Fe–N phases diagram (Fig. 8).

This fact predicts the formation of α-ferrite when γ'-Fe_4N nitride is slowly cooled from the eutectoid temperature 592 °C where the α+ γ'/γ' phase boundary presents the minimum value, i.e., this transformation allows the nitrogen flow from low-nitrogen α-ferrite to high-nitrogen γ'-Fe_4N nitride and is not accomplished until the nitrogen content of γ'-Fe_4N reaches its equilibrium value with respect to α-ferrite at a given temperature. To estimate the driving force, the evolution of the α+ γ'/γ' phase boundary as a function of temperature should be known.

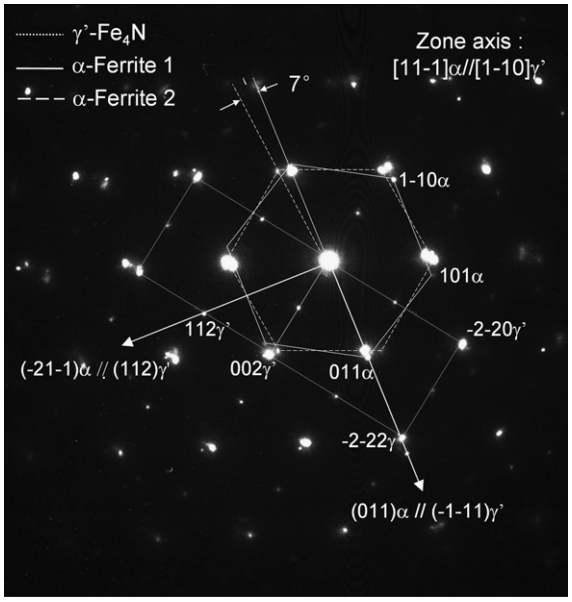

Fig. 7 – Electron diffraction pattern showing the Kurdjumov–Sachs orientation relationship between the acicular ferrite and the γ'-Fe_4N nitride. The arrows point out the characteristic parallelisms of this orientation relationship. Note that a second ferrite reflection net is related to the first one by a rotation of 7°.

As can be seen in the most recent calculated phase diagrams [17–19], the phase boundary varies from 5.68 wt.% (19.4 at.%) at 592 °C to 5.88 wt.% (20 at.%) at 214 °C. In addition, Kooi et al. [17] collected the experimental composition–temperature data reported by different authors and these were conflicting. The enormous discrepancies could be ascribed to experimental difficulties in determining the nitrogen content in γ'-Fe_4N nitride for the equilibrium between α-ferrite and γ'-Fe_4N [15]. In this study, effort was not made on using electron probe micro analysis to measure the α+ γ'/γ' phase boundary at different temperatures.

To the best of the authors' knowledge, Gerardin [14] is the only author who reported the formation of acicular α-ferrite in γ'-Fe_4N layer at the extreme surface of a nitrided iron specimen. The Bain orientation relationship between the two phases was found in his study.

In the present case, it is strongly suggested that acicular ferrite precipitates from pearlitic γ'-Fe_4N lamellae. A micrograph shown in Fig. 9 points out how this happens. It seems that acicular ferrite (whose length is about 100 nm) nucleates at the pearlitic α/γ' interfaces and its growth is limited by the adjacent pearlitic ferrite lamellae, because acicular and pearlitic ferrites don't necessarily have the same crystal orientation.

It is now necessary to explain how acicular ferrite in pearlitic γ'-Fe_4N lamellae shown in Fig. 9 turns into the state where γ'-Fe_4N lamellae become a whole block and acicular ferrite grows longer, as shown in Figs. 2 and 3. A mechanism was proposed by interpreting what was observed by Transmission Electron Microscopy.

A coarsened state of γ'-Fe_4N lamellae was presented in Fig. 10. At the middle of the micrograph, it is obvious that by coarsening [20–23], γ'-Fe_4N lamellae become 3 times thicker than those shown in Fig. 9 and consequently acicular ferrite (marked by arrows) could grow longer (but still within γ'-Fe_4N lamellae). At the left bottom the micrograph, one can see that the continuous coarsening of γ'-Fe_4N lamellae leads to a whole block in which pearlitic α/γ' interfaces completely disappear. Without these pearlitic α/γ' interfaces as obstacles, acicular ferrite could then grow as long as more than 1 μm (marked by a circle). This accords well with the observations shown in Figs. 2 and 3.

The passage form pearlitic structure to acicular structure is summarised in Fig. 11. In the Scanning Electron Micrograph (Fig. 11-a), three rectangular zones 1, 2 and 3, which reveal three

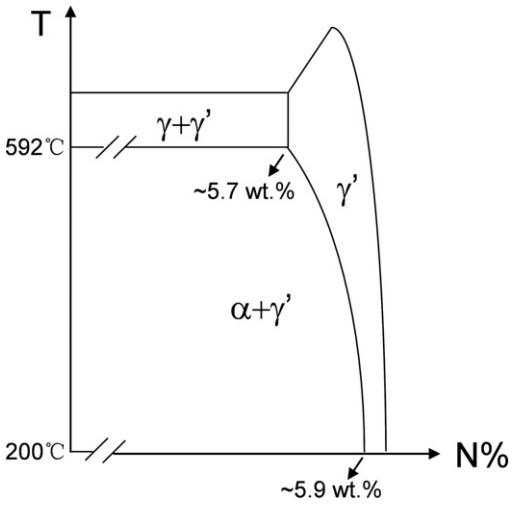

Fig. 8 – Schematic representation of the α+ γ'/γ' phase boundary in the Fe–N phases diagram.

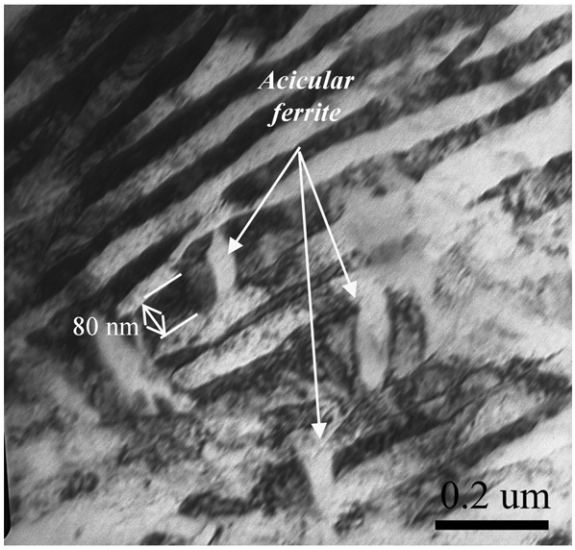

Fig. 9 – TEM micrograph showing the initial stage of the acicular ferrite precipitation (arrowed). Note that the growth of acicular ferrite is limited within the fine γ'-Fe_4N lamellae.

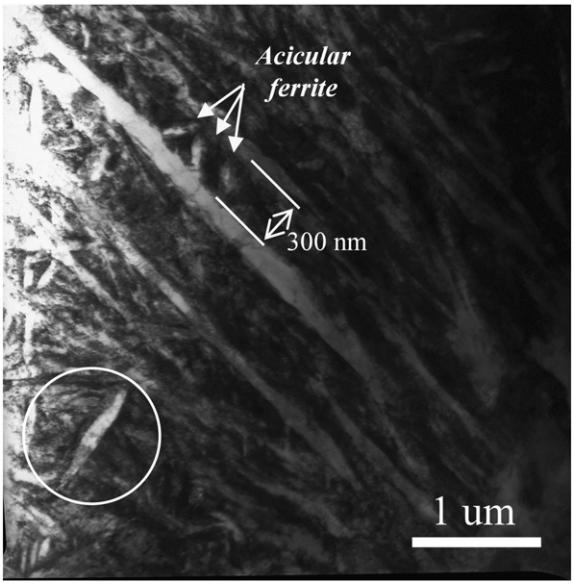

Fig. 10 – TEM micrograph showing acicular ferrite growing in coarsened γ'-Fe_4N lamellae (in the middle of the micrograph) and in large γ'-Fe_4N block (at the left bottom of the micrograph).

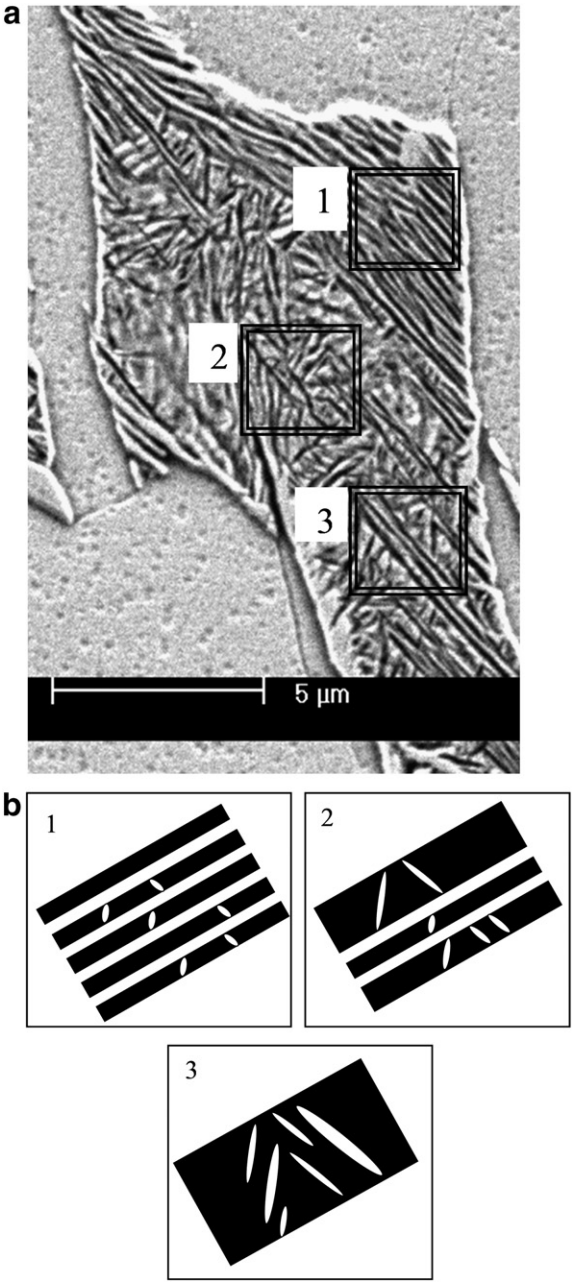

Fig. 11 – a) SEM micrograph and b) corresponding schematic representation of the acicular ferrite growth sequence. 3 rectangular zones correspond to 3 successive states respectively: (1) acicular ferrite grows in initially fine pearlitic γ'-Fe_4N lamellae, (2) in coarsened pearlitic γ'-Fe_4N lamellae and (3) in γ'-Fe_4N block.

different stages of the acicular ferrite formation respectively, are marked. In addition, three corresponding illustrations (Fig. 11-b) are provided for clarity:

Zone 1: due to the fact that the nitrogen content of γ'-Fe_4N, in equilibrium with ferrite, increases as the temperature decreases, acicular ferrite precipitates in pearlitic γ'-Fe_4N lamellae and its growth is limited by adjacent pearlitic ferrite;

Zone 2: as the cooling rate is very low, some pearlitic γ'-Fe_4N lamellae continue to coarsen and acicular ferrite has the possibility to grow longer. This intermediate stage could be seen in zone 2 of the Scanning Electron micrograph, in which fine and coarse γ'-Fe_4N lamellae coexist and acicular ferrite is visible in the latter.

Zone 3: the continuous coarsening of pearlitic γ'-Fe_4N lamellae leads to large γ'-Fe_4N blocks in which acicular ferrite can grow "freely" and a macroscopically acicular structure forms. It is clear that in zone 3 of the Scanning Electron micrograph, no more lamellar structure is visible and acicular structure dominates.

In order to better understand the formation of this acicular structure, isothermal holding on nitrogen pearlite, at different temperatures and for different holding time, should be further envisaged.

It is of great interest to exam the influence of acicular ferrite precipitation on the mechanical properties of nitrogen pearlite.

5. Conclusion

Acicular structure was observed on a Fe–N hypoeutectoid pearlitic alloy. Electron microdiffraction was employed to identify phases and conclusion was drawn that this acicular structure is in fact acicular α-ferrite precipitated in γ'-Fe_4N nitride.

Acicular ferrite develops, both the Nishiyama–Wassermann and Kurdjumov–Sachs orientation relationships, with γ'-Fe_4N nitride. The shapes of acicular ferrite, lens-like and platelet-like, corresponding to N–W and the K–S orientation relationships respectively, are in accord with the symmetry theory.

The passage from lamellar pearlitic structure to acicular structure was proposed. The driving force for acicular ferrite precipitation from γ'-Fe_4N nitride was supposed to be the fact that nitrogen content of γ'-Fe_4N, in equilibrium with α-ferrite, increases as the temperature decreases. Acicular ferrite growth is limited by adjacent pearlitic ferrite. The formation of acicular structure is caused by coarsening of pearlitic γ'-Fe_4N lamellae and formation of large γ'-Fe_4N nitride block.

Acknowledgement

The authors greatly acknowledge the financial support of the ArcelorMittal SA.

REFERENCES

[1] Hillert M, Jarl M. A thermodynamic analysis of the iron–nitrogen system. Metall Trans A 1975;6:553–9.
[2] Ågren J. A thermodynamic analysis of the Fe–C and Fe–N phase diagrams. Metall Trans A 1979;10:1847–52.
[3] Kunze J. Thermodynamic calculation of phase diagrams in the iron–nitrogen system. Steel Research 1986;57:361–7.
[4] Wriedt HA, Gokcen NA, Nafziger RH. The Fe–N (iron–nitrogen) system. Bulletin of Alloy Phase Diagrams 1987;8:355–77.
[5] Kunze J. Nitrogen and carbon in iron and steel; thermodynamics, first ed., Berlin: Akademie-Verlag; 1990.
[6] Bose BN, Hawkes MF. Eutectoid transformation in alloys of iron and nitrogen. Trans AIME 1950;188:307–16.
[7] Bell T, Farnell BC. Transformation of iron–nitrogen austenite to pearlite. International symposium on metallurgical chemistry-Applications in ferrous metallurgy. Sheffield; 1971. p. 275–7.
[8] Xiong XC, Redjaïmia A, Gouné M. Pearlite in hypoeutectoid iron–nitrogen binary alloys. J Mater Sci 2009;44: 632–8.
[9] Morniroli JP, Steeds JW. Microdiffraction as a tool for crystal structure identification and determination. Ultramicroscopy 1992;45:219–39.
[10] Redjaïmia A, Morniroli JP. Application of microdiffraction to crystal structure identification. Ultramicroscopy 1994;53: 305–17.
[11] Cahn JW, Kalonji G. Symmetry in solid state transformation morphologies. International Conference on Solid-Solid Phase Transformations. Pittsburgh: The Metallurgical Society of AIME; 1981. p. 3–14.
[12] G.L. Kalonji, Symmetry principles in the physics of crystalline interfaces, in, Massachusetts Institute of Technology, 1982.
[13] Jack DH, Jack KH. Invited review: carbides and nitrides in steel. Mater Sci Eng 1973;11:1–27.
[14] D. Gerardin, Study of structure faults and phase transformations of iron carbonitrides (in French), in, Institut National Polytechnique de Lorraine, 1978.
[15] Somers MAJ, van der Pers NM, Schalkoord D, Mittemeijer EJ. Dependence of the lattice parameter of iron nitride Fe4N1-x on nitrogen content; accuracy of the nitrogen absorption datairon nitride Fe4N1-x on nitrogen content; accuracy of the nitrogen absorption data. Metall Trans A 1989;20:1533–9.
[16] De Wit L, Weber T, Custer JS, Saris FW. Thermodynamic stability of iron nitrides at temperatures below 350 °C. Phys Rev Lett 1994;72:3835–8.
[17] Kooi BJ, Somers MAJ, Mittemeijer EJ. An evaluation of the Fe–N phase diagram considering long-range order of N atoms in γ'-Fe4N1-x and ε-Fe2N1-z. Metall Mater Trans A 1996;27: 1063–71.
[18] Du Marchie EH, van Voorthuysen NC, Chechenin DO Boerma. Low-temperature extension of the Lehrer diagram and the iron–nitrogen phase diagram. Metall Mater Trans A 2002;33: 2593–8.
[19] Liapina T, Leineweber A, Mittemeijer EJ. Phase transformations in iron-nitride compound layers upon low-temperature annealing: diffusion kinetics of nitrogen in ε- and γ'-iron nitrides. Metall Mater Trans A 2006;37:319–30.
[20] Livingston JD, Cahn JW. Discontinuous coarsening of aligned eutectoids. Acta Metall 1974;22:495–503.
[21] Hillert M. The formation of pearlite. In: Zackeay VF, Aaronson HI, editors. Decomposition of austenite by diffusional processes, Interscience; 1962.
[22] Chen JK, Spencer CW, Ekstrand ME, Chen G, Reynolds Jr WT. Eutectoid decomposition in Ag-Ga. Metall Mater Trans A 1996;27:1683–9.
[23] Ardell AJ. Microstructural stability at elevated temperatures. J Eur Ceram Soc 1999;19:2217–31.